Influences of alkali fluxes on direct reduction of chromite for ferrochrome production

by D. Paktunc*, Y. Thibault*, S. Sokhanvaran*, and D. Yu*

Synopsis

Prereduction and flux-aided direct reduction of chromite provide significant advantages in reducing energy consumption and greenhouse gas emissions during ferrochrome production. In this investigation, a comparative evaluation of the influences of several alkali fluxes was carried out based on experimental observations supplemented by advanced material characterization and thermodynamic predictions. Direct reduction of a chromite ore with alkali fluxes at 1300°C for 1 hour produced $(Cr,Fe)_7C_3$ type alloys with Cr/Fe mass ratios from 0.7 to 2.3. Among the alkali fluxes, reduction aided by NaOH resulted in a high degree (85%) of Cr metallization with the ferrochrome alloy being $Cr_{4.2-4.6}Fe_{2.4-2.8}C_3$. The formation of liquid slag, which facilitated Cr metallization, was limited by the formation of $NaAlO_2$ between 800 and 1300°C. This, in turn, restricted the collection and transport of the charged ionic Cr species (*i.e.* O^{2-}) to graphite particles. Under the conditions studied, ferrochrome particles were often small and largely unliberated, which would make the physical recovery of ferrochrome challenging. At 1400°C, the amount of liquid slag increased, enabling the growth of alloy particles. Direct reduction of chromite aided by NaOH is promising as an alternative technology to conventional flux-based smelting in electric arc furnaces.

Keywords

chromite, ferrochrome, direct reduction, prereduction, smelting, carbothermic reaction, alkali flux.

Introduction

Conventional smelting processes are energy-intensive (Riekkola-Vanhanen, 1999) with the energy requirements greater than 4 MWh/t (Naiker and Riley, 2006; Beukes, van Zyl, and Neizel, 2015), and the greenhouse gas emissions can be significant, exceeding 10.5 t CO_2 per ton Cr in ferrochrome produced (International Chromium Development Association, 2016). These include emissions occurring on-site (smelter), emissions due to electricity production, and emissions due to upstream processes. Overall energy requirements are influenced by the degree of prereduction and smelter charge temperature. Significant reduction in electricity consumption can be realized if the charge is prereduced before feeding to the submerged arc furnace (Niayesh and Fletcher, 1986). This consideration has led to the development of several prereduction technologies, with the most important example being the Premus

process. In comparison to the conventional smelting processes, this prereduction process lowers the overall energy consumption and greenhouse gas emissions by about one-third (Naiker, 2007).

Prereduction of chromite with the use of various fluxes or additives has been the topic of many studies over at least three decades. The additives tested since 1986 include borates, NaCl, NaF, and CaF_2 (Katayama, Tokuda, and Ohtani, 1986), CaF_2 and NaF (Dawson and Edwards, 1986), K_2CO_3, CaO, SiO_2, Al_2O_3, and MgO (van Deventer, 1988), granite and CaF_2 (Nunnington and Barcza, 1989), SiO_2 (Weber and Eric, 1992; Lekatou and Walker, 1997), Portland cement, lime, and SiO_2 (Takano *et al.*, 2007), CaO and SiO_2 (McCullough *et al.*, 2010), $CaCO_3$ (Neizel *et al.*, 2013), and MgO, CaO, SiO_2 and Al_2O_3 (Wang, Wang, and Chou, 2015). Since the filing of the patent application on the use of several alkalis as the accelerants (Winter, 2015; Barnes, Muinonen, and Lavigne, 2015), we have been performing systematic studies to improve our understanding of the roles of various fluxes. Our studies involved using NaCl, NaOH, Na_2CO_3, $CaCl_2$, Ni, and a metallurgical waste product as the fluxes in accelerating the reduction of chromite and developing a fundamental understanding of the kinetics and mechanisms of reduction and metallization (Sokhanvaran and Paktunc, 2017, 2018; Sokhanvaran, Paktunc, and Barnes, 2018; Yu and Paktunc, 2017; Yu and Paktunc, 2018a, 2018b, 2018c). These studies formed parts of the broader research into improving and optimizing the conventional smelting processes as well as developing new reduction technologies to reduce energy demands and greenhouse gas emissions, and evaluating the

---

* *CanmetMINING, Natural Resources Canada, Canada.*

Influences of alkali fluxes on direct reduction of chromite for ferrochrome production

development of direct reduction of chromite as an alternative ferrochrome production technology. Direct reduction of chromite can be defined as the production of ferrochrome from chromite ore using a carbon reductant but without melting/reduction in electric arc furnaces. Although direct reduction of iron is well known and widely practiced as an industrial process for producing pig iron, direct reduction of chromite has not been tested until recently. The SRC process developed in Japan in the 1970s can be considered direct reduction if it is used as a stand-alone process. Previous studies considered the use of various fluxes in a prereduction process prior to smelting in electric arc furnaces and as such, they differ in philosophy from the direct reduction process. In this paper, we present our study results in a comparative manner to illustrate the influence of the three alkali compounds in the direct reduction of chromite.

Materials and methods

An ore sample from the Black Thor deposit from the Ring of Fire area in northern Ontario was ground and sieved to −106+75 μm size range. The ore, with a grade of 43.12 wt% Cr_2O_3 and Cr/Fe ratio of 1.97 (21.4 wt% Fe_2O_3), was blended with graphite as the reductant and an alkali flux (NaCl, NaOH, or Na_2CO_3) in the proportions of 100:22:12 (by weight) unless otherwise indicated in the text. The ore contained 84 wt% chromite, with an average composition of $(Mg_{0.4}Fe_{0.6})(Cr_{1.3}Al_{0.5}Fe_{0.1})O_4$, and 16 wt% clinochlore with the average formula of $Si_{6.0}Al_{3.3}Cr_{0.5}Mg_{9.9}Fe_{0.2}O_{20}(OH)_{16}$ based on ModAn estimates (Paktunc, 2001). The mixture was homogenized prior to the experimental studies.

The experiments were performed in a sealed vertical tube furnace with $MoSi_2$ heating elements. The sample, weighing 60 g, was placed in an alumina crucible suspended in the furnace by a tungsten wire and the tests were conducted at 1100 and 1300°C for periods of 45 and 60 minutes under Ar atmosphere at a flow of 900 mL/min. Following reduction, the crucible was raised to the upper zone of the furnace and cooled in Ar. Off-gases were continuously analysed by an infrared gas analyser.

The samples were also subjected to thermogravimetry and differential scanning calorimetry (TG-DSC) analyses under Ar atmosphere with continuous gas analysis. TG-DSC analysis was performed using a NETZSCH STA 449C simultaneous thermal analyser coupled to a NETZSCH QMS 403C Aeolos mass spectrometer. For each test, a sample of 42 mg was placed inside an alumina crucible before loading it into the TG-DSC. After closing the top of the instrument, the atmosphere surrounding the crucibles inside the TG-DSC was purged with a vacuum to remove air. A controlled flow of ultra-high purity argon was introduced and maintained as an inert carrier gas for the duration of each test. The sample was quickly heated from room temperature to 700°C, followed by heating at 10°C/min to the target temperature and held for a specified time before being rapidly cooled to room temperature under argon atmosphere.

The products formed during carbothermic reduction in the sealed tube furnaces were characterized by X-ray diffraction, optical microscopy, scanning electron microscopy, and electron microprobe analysis and, at the molecular-scale, by synchrotron-based X-ray techniques. Electron microprobe analysis (JEOL JXA-8900) involved wavelength-dispersive X-

ray microanalysis on polished sections at an accelerating voltage of 20 kV. Individual quantitative analyses were done using a probe current of 10 to 35 nA and counting times ranging from 10 up to 60 seconds on peak and background. Na Kα X-ray intensity was monitored as a function of time to ensure that there was no Na mobility under the analytical conditions used. Estimation of the distribution of Fe^{3+} and Fe^{2+} in the chromite analyses was based on stoichiometry to balance the charge from the ideal spinel formula $(Mg,Fe^{2+})(Cr,Al,Fe^{3+})_2O_4$. Carbon concentration in the metallic phase was determined by difference from a total of 100%, an approach consistent for crystalline M_7C_3 type carbides. Matrix corrections were made using the $\Phi(\rho z)$ program provided by JEOL to take into considerations matrix effects introduced by compositional differences between the unknowns and standards.

Mineral quantities and liberation were determined using a TESCAN Integrated Mineral Analyzer (TIMA) equipped with four silicon-drifted energy-dispersive X-ray detectors. The analyses were done at an accelerating voltage of 25 kV and a beam current of 5.5 nA using the high-resolution mapping mode with a step size of 0.5 μm.

Synchrotron-based X-ray absorption near-edge spectroscopy (XANES) spectra were collected at bending magnet and insertion device beamlines. Bulk XANES spectra were collected in transmission mode on finely ground samples spread onto tape as monolayers. Micro-XANES spectra were collected using a 2 μm beam and confocal microchannel array optics. The confocal method provides 2–5 μm depth resolution and limits detection of emissions to small volumes of materials at specified depths along the path of the focused beam through the sample. Data reduction and analysis were done by ATHENA (Ravel and Newville, 2005) and the least-squares fitting analyses of the XANES spectra were performed with LSFitXAFS (Paktunc, 2004).

In support of the experimental and characterization studies, thermodynamic simulations were performed using FactSage with the input parameters being identical to those of the experimental studies (*i.e.* mass proportions of ore:graphite:flux being 100:22:12 and the ore composed of 84 wt% chromite and 16 wt% clinochlore).

Results

Thermogravimetry and differential scanning calorimetry tests

TG-DSC tests in the absence of a flux indicated that the first thermal event took place at approximately 700°C, resulting in the appearance of an endotherm as well as about 3 wt% mass loss (Figure 1). Off-gas analysis by mass spectrometry indicated the formation of gaseous H_2O from this thermal event. This is likely to be resulting from the loss of structural water from clinochlore. No appreciable amount of reduction took place before 1100°C. The reduction rate became significant when the temperature reached 1300°C, resulting in a rapid mass loss. The main gas product was CO, based on the off-gas analysis. To allow for an unambiguous comparison with the other tests, the thermogravimetry (TG) curve was reprocessed by separating the two thermal events (*i.e.* loss of structural water and reduction), and normalizing the mass loss to represent the mass loss per 100 mg ore. The
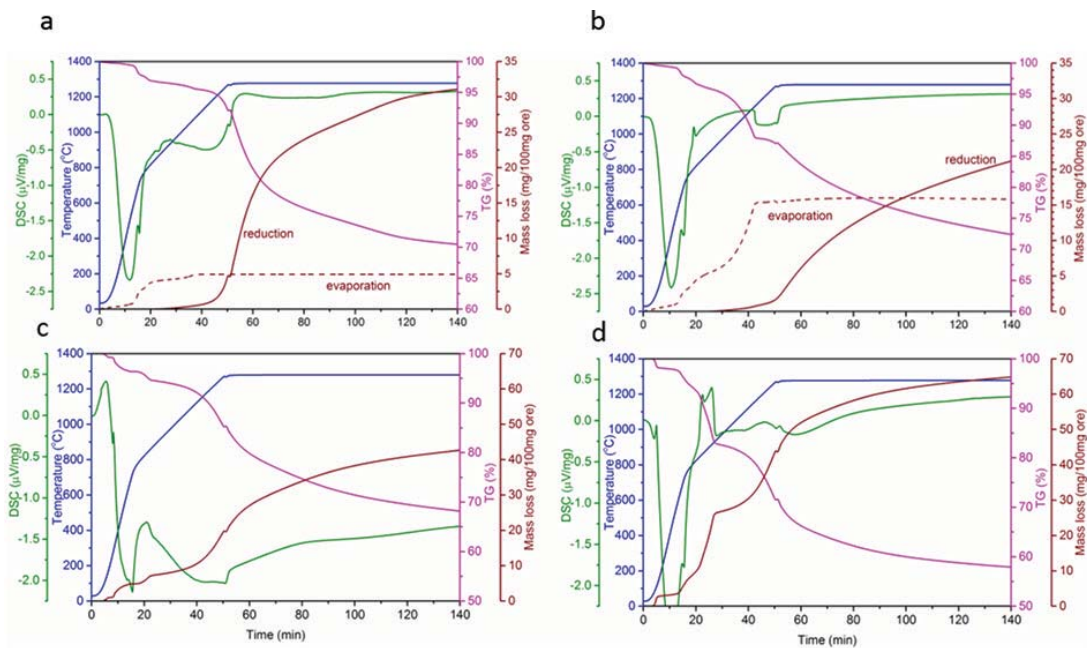
Figure 1—TG-DSC analysis of the reduction of chromite at 1300°C (a) without a flux, (b) with 12 wt% NaCl, (c) with 12 wt% NaOH, and (d) with 32 wt% Na$_2$CO$_3$. DSC: differential scanning calorimetry; TG: thermogravimetry

mass loss curves for both the thermal dehydration and reduction (Figure 1a) indicate that the carbothermic reduction of chromite was not complete after 2 hours of reduction.

TG-DSC test results evaluating the effect of NaCl addition on the carbothermic reduction are shown in Figure 1b. The same thermal dehydration event described earlier for the no-flux case also took place in this test, as indicated by the mass loss and an endotherm at about 700°C. A second endotherm was identified at approximately 800°C, representing the melting of NaCl. Significant evaporation of the molten NaCl took place with an increase in temperature, resulting in continuous mass loss. The evaporation of NaCl was complete when the temperature reached about 1150°C, marked by the sudden change of the slope of the TG curve and a rapid decrease of the DSC signal. Based on off-gas analysis, the contributions of dehydration, evaporation of molten NaCl, and reduction to the mass loss were evaluated. The curve representing the mass loss due to reduction was calculated by re-processing the TG curve (Figure 1b). A comparison of the results to those of the no-flux case suggests that the addition of NaCl inhibited the carbothermic reduction of chromite to a certain degree.

TG-DSC tests in the presence of NaOH produced a DSC signal that is different from the ones observed with NaCl and without a flux. As illustrated in Figure 1c, the first endotherm appeared at temperatures above 100°C with about 2 % mass loss. The appearance of gaseous H$_2$O from the off-gas analysis indicates that this thermal event is due to the evaporation of absorbed water from NaOH. The second endotherm occurred at approximately 300°C, resulting from the melting of NaOH. A second stage of mass loss was observed in association with the melting of NaOH. The increase in the H$_2$O peak at this stage can be explained by the mass loss resulting from the decomposition of NaOH to Na$_2$O and H$_2$O. The third stage of mass loss is linked with an

endotherm on the DSC curve and an increase in CO in the off-gas analyses that occurred at 700°C. A reaction between Na$_2$O and C forming CO gas (Sokhanvaran, Paktunc, and Barnes, 2018), in addition to the decomposition of clinochlore and reduction of Fe, could be responsible for this change. Reduction reactions progressed aggressively above 1100°C resulting in a major mass loss (Figure 1c). Mass losses corresponding to about 38% of the ore occurred during the latter stages of the test.

The effect of Na$_2$CO$_3$ on carbothermic reduction was investigated by mixing chromite and graphite with 32% Na$_2$CO$_3$ (Figure 1d). The first thermal event occurred above 100°C, resulting from the evaporation of absorbed water in the sample, similar to that observed in the case of NaOH (Figure 1c). The second endotherm appeared at 700°C in association with a new water peak. This phenomenon, which is similar to those observed with NaCl flux and with no flux (Figure 1a and 1b), is linked to the dehydration of clinochlore. The third endotherm on the DSC curve appeared around 800°C. This change is probably a result of the reaction of Na$_2$CO$_3$ with C to form CO gas and Na vapour. Melting of Na$_2$CO$_3$ occurred at 850°C, resulting in an increase in the rate of mass loss. Reduction of chromite occurred during the last stage, which is confirmed by the CO in the off-gas analyses. Similar to the case with NaOH, isolation of the different mass losses is impossible due to the interactions between carbonate and graphite. The mass loss during the final stage was about 38% of the ore, which is similar to that observed in the NaOH case.

Carbothermic reaction products

Representative backscattered electron photomicrographs of the products that formed after 1 hour of reduction at 1300°C are shown in Figure 2. The ore reduced in the presence of NaCl displays some similarities to that reduced with no flux.

Influences of alkali fluxes on direct reduction of chromite for ferrochrome production
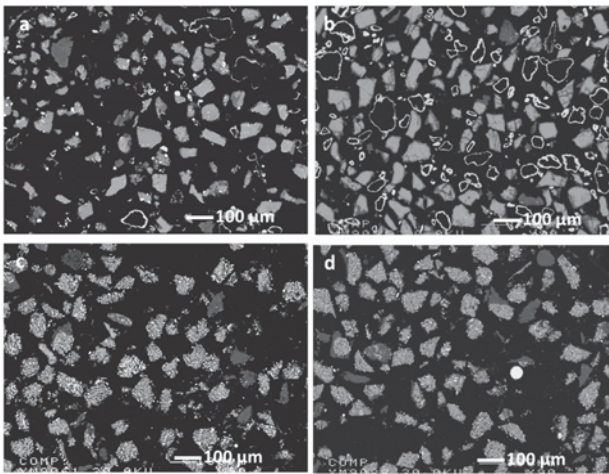

Figure 2—Backscattered electron photomicrographs of the products that formed after 1 hour of reduction at 1300°C (a) in the absence of a flux, (b) with NaCl , (c) with NaOH, and (d) with Na₂CO₃. Alloy or metal particles appear as white or very light grey, the residual chromite grains occur as light grey, and the slag as dark grey domains. Spherical white particle in (d) is an Fe-rich metal droplet measuring about 40 μm across

Both are characterized by a lower degree of metallization in terms of Fe and Cr and the occurrence of alloy particles as rings on the residual graphite particles. In contrast, the products that formed in the presence of NaOH and Na_2CO_3 display higher degrees of metallization with increased amounts of alloy particles.

The compositions of the products as determined by powder XRD and scanning electron microscopy include chromite, graphite, and Cr-Fe carbides in all the samples formed after 1 hour of carbothermic reaction. Forsterite (Mg_2SiO_4) is present in the products that resulted in the presence of NaCl and Na_2CO_3.

Chromite grains in the original ore display zoning developed along particle margins and microfractures. The zoning is primary as observed in the original ore due to a geological event that affected the chromite deposits and the host rocks. The electron microprobe analyses indicate that the rims have much higher Cr contents and slightly lower Mg in the tetrahedral sites in comparison to the original (pre-metamorphic event) chromite compositions reflected by the chromite core compositions (Figure 3). The zoning, with higher Cr and lower Al in the octahedral sites and slightly increased Mg fractions in the tetrahedral sites, is one of the characteristics of the Ring of Fire chromite, and is believed to play an important role in the reducibility of the ores. This feature will be discussed in detail in a separate paper.

The compositions of the chromite reduced in the presence of NaCl after 45 minutes' reaction are similar to the original chromite compositions, indicating that very little or no detectable chemical changes occurred. The sample reduced for 60 minutes in the presence of NaCl displayed some changes in the chromite composition although some residual chromite particles remained intact. Compositional changes are essentially the same, limited to reduced Fe^{2+} contents (or increased Mg at the expense of Fe^{2+}) due to removal of iron from the crystal structure.

The residual chromite grains in the products of the NaOH and Na_2CO_3 experiments have virtually no Fe remaining (Figure 3). The zoning in chromite is less apparent. The lighter grey areas in Figures 4a–c represent residual chromite, whereas the darker grey domains represent the slag. The residual chromite grains in both cases, represented by lighter grey areas in Figures 4a–c, are depleted in Fe (both divalent and trivalent) and the Cr and Al contents are variable.

Metallization and composition of alloys

The compositions of the ferrochrome alloys formed under the influence of NaCl flux are shown in Figure 5. There are two compositional types: one that occurs along intergrain boundaries and crystallographic planes of the host chromite as shown in Figure 4d; and a second, which is essentially an Fe metal with minor Cr and carbon. The latter type is an M_7C_3 type carbide with a variable composition from $Cr_{3.2}Fe_{3.8}C_3$ to $Cr_{5.0}Fe_{2.0}C_3$ (Figure 5). The M_7C_3 type occurs as rings on residual graphite particles (Figure 2b).

Ferrochrome alloys formed with NaOH flux appear to have a tighter compositional variation along the M_7C_3 join (Figure 5). The composition is variable from $Cr_{4.2}Fe_{2.8}C_3$ to $Cr_{4.6}Fe_{2.4}C_3$. Ferrochrome particles in larger domains of slag tend to be coarser (Figure 4a) than those developing from within the chromite grains (Figure 4b). Another mode of occurrence of the alloy particles is in the form of blebs or metal droplets that are rich in Fe. In the example shown in Figure 4e, an Fe-rich M_7C_3 phase ($Cr_2Fe_5C_3$) occurs as an exsolved phase from the Fe metal.

The alloys formed in the presence of Na_2CO_3 flux have compositions variable from $Cr_3Fe_4C_3$ to $Cr_4Fe_3C_3$ (Figure 5). The carbide occurs along the particle rims of the residual chromite as well as developing along the crystallographic planes of the host (Figure 4c). Its occurrence is similar to that formed in the presence of NaOH flux (Figures 4a and 4b).
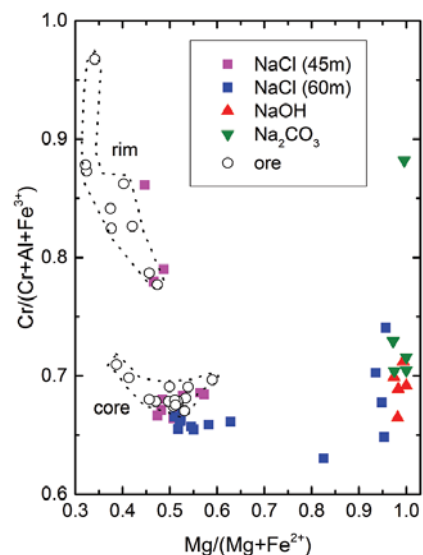

Figure 3—Electron microprobe analyses of the original and residual chromite particles in terms of cation fractions in the tetrahedral and octahedral sites of chromite. Original chromite is denoted as 'ore'. Other chromite types are residual chromite formed at 1300°C after 60 minutes of carbothermic reaction in the presence of NaCl, NaOH, and Na₂CO₃. NaCl (45m): 45 minutes' reaction

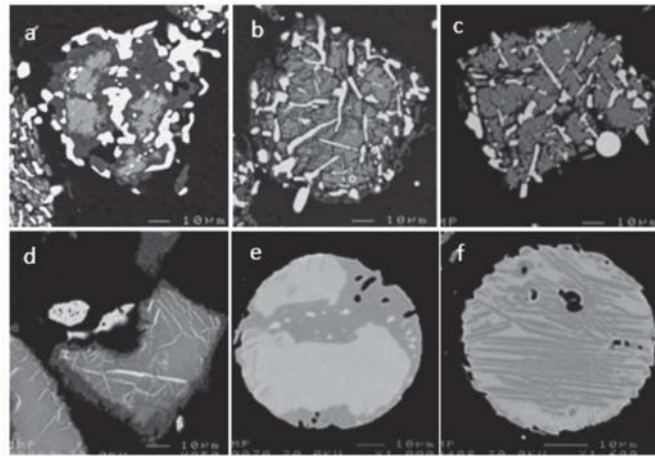# Influences of alkali fluxes on direct reduction of chromite for ferrochrome production

Figure 4—Backscattered electron photomicrographs of residual chromite particles in the presence of NaOH flux (a and b), Na_2CO_3 flux (c), and NaCl flux (d). Light grey areas in (a) and (b) are residual chromite, dark grey domains are slag, and white particles are alloy. Exsolution lamellae (white) in (d) are Fe_9Cr formed *in situ* within chromite (grey). Iron melt droplets (white) with exsolved $Fe_{19-21}Cr_{2-4}C_6$ (grey) formed in the presence of NaOH flux (e) and Na_2CO_3 flux (f). Scale bar is 10 µm in all
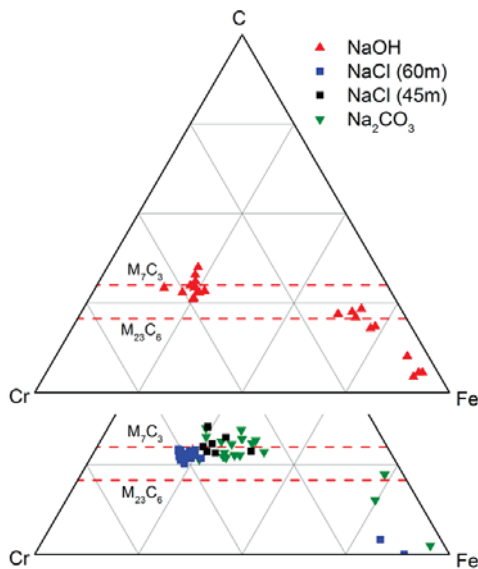

Figure 5—Composition of the metallic phases, determined by electron microprobe, formed in the presence of NaOH (top), and NaCl and Na_2CO_3 (bottom). Iron-rich particles with low Cr and C are those that formed either *in situ* in chromite (Figure 7d) and as melt droplets (Figures 7e and 7f). Compositions of the M_7C_3 type carbides formed with NaOH can be defined as $Cr_{4.2-4.9}Fe_{2.1-2.8}C_3$, with NaCl flux as $Cr_{3.2-5.0}Fe_{2.0-3.8}C_3$, and with Na_2CO_3 flux as $Cr_{3-4}Fe_{3-4}C_3$. NaCl (45 m: 45 minutes reaction)

XANES spectra collected at the Cr and Fe K-edges are shown in Figure 6. In terms of Cr reduction, least-squares fitting of the spectrum representing no-flux conditions indicates that the degree of Cr metallization is only 36% after 1 hour of reduction at 1300°C, while Fe metallization is complete at 100% (Figure 6). Reduction of Fe much earlier than Cr is also evident from the empirical evidence shown by TGA-DSC analyses, furnace tests, and thermodynamic predictions. Addition of NaCl as the flux resulted in a slightly improved metallization at 45% after 1 hour of reduction. In terms of Fe reduction, addition of NaCl as the flux slightly

degraded the metallization. The degree of metallization is 85% for Cr and 100% for Fe with the use of NaOH as the flux. This is significant in comparison to the degree of Cr metallization reached in the absence of a flux, approximately 36%. A lower degree of Cr metallization at 66% and 100% Fe metallization were achieved with Na_2CO_3 as the flux. In general, the results indicate various degrees of reduction and metallization, with Fe reduction always preceding that of Cr.

Slag composition

Electron microprobe analyses indicate that the slags formed in the presence of NaOH and Na_2CO_3 are dominated by SiO_2, Al_2O_3, Na_2O, and MgO. In contrast, as illustrated on the Na_2O-Al_2O_3-SiO_2 phase diagram representing 1300°C and 1 atm. (Figure 7), the slag formed in the presence of NaCl contains very little Na.

Slag that formed from reduction in the presence of NaOH is represented by material near the residual chromite particles as shown on the backscattered electron photomicrograph (Figure 7). It plots in or near the slag-liquid+$NaAlO_2$ field. Only a few points at the outer edges of the 'slag' plot in the slag-liquid field. Those that are away from the residual chromite, such as the one marked as '2' on the backscattered electron photomicrograph, plot in the slag-liquid field (Figure 7). The MgO content is high at 16.64 wt% in comparison to that near a chromite particle (4.92 wt%). The slag contains minor amounts of Cr_2O_3 with values of 0.92 wt% near a residual chromite particle and 0.38 wt% in an isolated slag particle.

Slag formed with Na_2CO_3 displays some similarities to that with NaOH. However, the 'slag' materials appear to have a bimodal distribution: one plotting in the $NaAlO_2$+$NaAl_9O_{14}$ field and the other largely in the slag-liquid field.

Speciation of chromium

In order to understand the mechanism of Cr release to the molten slag, we determined the speciation of Cr in slag using a focused X-ray beam and confocal optics, allowing detection of emissions from small volumes of material at specified depths. One of the samples represents reduction at 1300°C

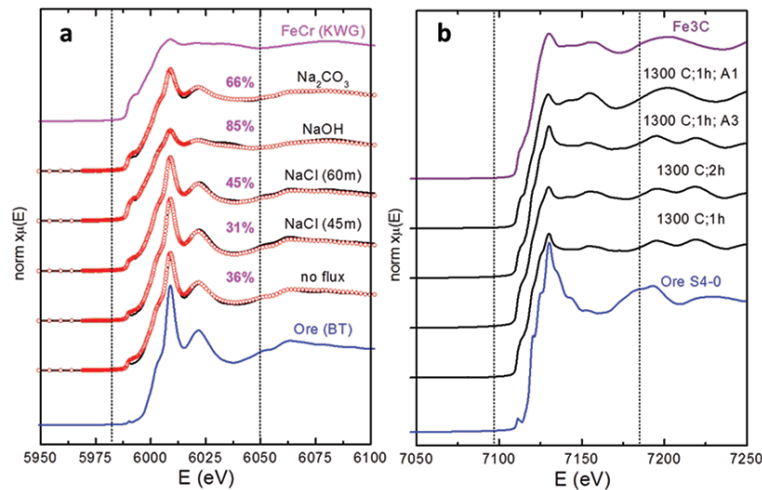# Influences of alkali fluxes on direct reduction of chromite for ferrochrome production

Figure 6—XANES spectra of the products formed. Normalized k^3-weighted Cr K-edge spectra are on the left and Fe K-edge spectra on the right. The degrees of Cr metallization (left) are based on least-squares fitting of the reference spectra of ferrochrome (FeCr, in fuschia) and chromite ore (ore, in blue) in the energy range marked by vertical lines at approximately 5982 and 6050 eV. Solid black lines are experimental spectra, whereas the lines with red circles are simulated spectra
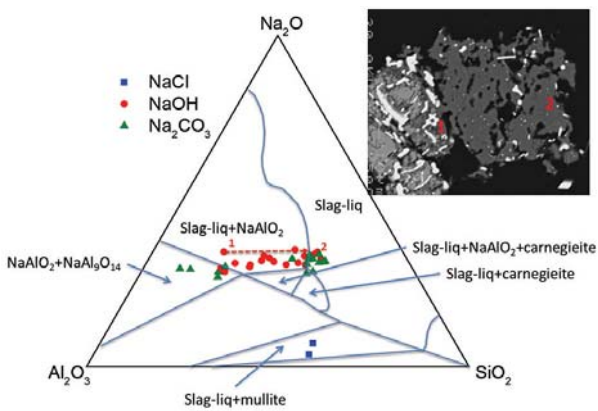

Figure 7—Na_2O-Al_2O_3-SiO_2 phase diagram representing 1300°C and 1 atm. with slag compositions of the products resulting from reduction with the alkali fluxes. Slag domains are dark grey on the backscattered electron photomicrograph representing material from the NaOH experiment. The numbers refer to slag adjacent to the residual chromite particle (1) and slag that is at a distance (2). Carnegieite: $NaAlSiO_4$; mullite: $2Al_2O_3 \cdot SiO_2$

without a flux (Figure 8). A residual chromite particle rimmed with minute Fe-rich alloy particles along the particle surface displays concentric zoning with decreased Cr and very low Fe in its outer zone. Micro-XANES spectra collected from these zones (labelled with '1-1' and '1-3' in Figure 8c) indicate identical Cr speciations that are typical of the chromite structure. Another zoned chromite particle with no Fe remaining in its outer rim (labelled '3' and '4' in Figure 8c) and adjacent to a large Cr-rich ferrochrome alloy particle (labeled '2') is also dominated by Cr^{3+} species. In other words, Cr is trivalent and octahedrally coordinated to oxygen atoms across the residual chromite particle, irrespective of the zoning, and there are no intermediary species between the trivalent and zero-valent species. These results are conclusive, since the micro-XANES spectra are collected from very small volumes within the particles, and as such they are not influenced by emissions from adjacent zones.

Another sample representing reduction with NaOH at 1100°C for 1.5 hours was studied with the aim of determining Cr speciation of the slag, which is dominated by $Na(Cr,Al,Fe)O_2$. Based on electron microprobe analyses of 15 grains, its composition can be defined as $Na_{0.9-1.2}Cr_{0.2-0.5}Al_{0.3-0.5}Fe_{0.0-0.3}O_2$. It occurs with a Na-Mg-Al silicate and residual chromite, which is $MgCr_{1.4}Al_{0.6}O_4$ and similar to the species illustrated in Figure 3. Micro-XANES spectra from the slag indicate that Cr occurs as trivalent species and that it is octahedrally coordinated to oxygen (Figure 9).

Beneficiation and recovery of ferrochrome alloys

Equally important in the direct reduction process are the physical separation and recovery of ferrochrome particles from the slag. This requires that the ferrochrome particles are coarse and that they are liberated when ground to a particle size range that is suitable for conventional gravity and/or magnetic mineral processing techniques.

The distribution of the ferrochrome particles and their degree of liberation were determined by automated mineralogy techniques, in which the particles are identified chemically and their quantities along with their liberation are measured. Shown in Figure 10 are backscattered electron images of the particles and their colour-coded representation. These are particles formed after 1 hour of direct reduction with NaOH at 1300°C. In general, the ferrochrome alloy particles are smaller than 20 μm. It appears that the ferrochrome alloy particles tend to occur as larger particles, around 20 μm in size, where the associated slag phase is coarse.

Between 20 000 and 30 000 such particles were measured by the quantitative or automated mineralogy technique (Figure 11). In the case of NaOH flux, ferrochrome alloy particles constitute about 26% by volume of the total particles. The slag constitutes about 50%, and the residual chromite 22%. The amount of ferrochrome particles is significantly underestimated because the spatial resolution of the technique is limited in detecting and counting small

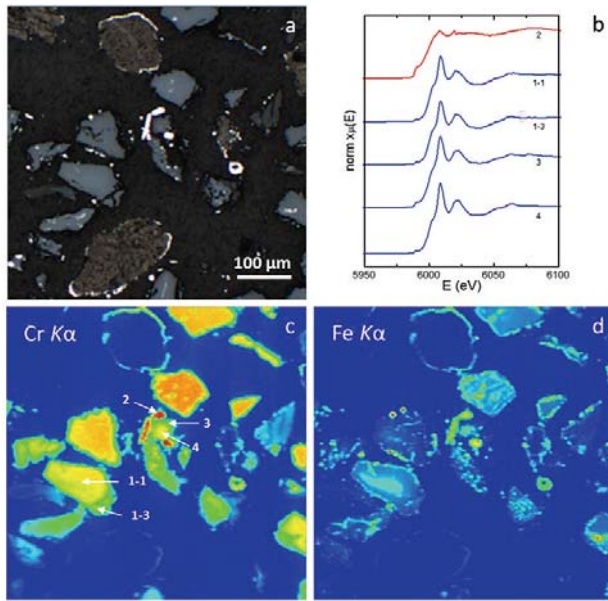# Influences of alkali fluxes on direct reduction of chromite for ferrochrome production

Figure 8—Backscattered electron image of (a) normalized k³-weighted Cr K-edge micro-XANES spectra from locations shown in (c), and (b) corresponding micro-X-ray fluorescence maps of Cr (c) and Fe (d) of the sample reduced at 1300°C for 1 hour without a flux. The maps represent several micrometer-thick sections, collected using microchannel confocal optics and show the locations of micro-XANES spectra
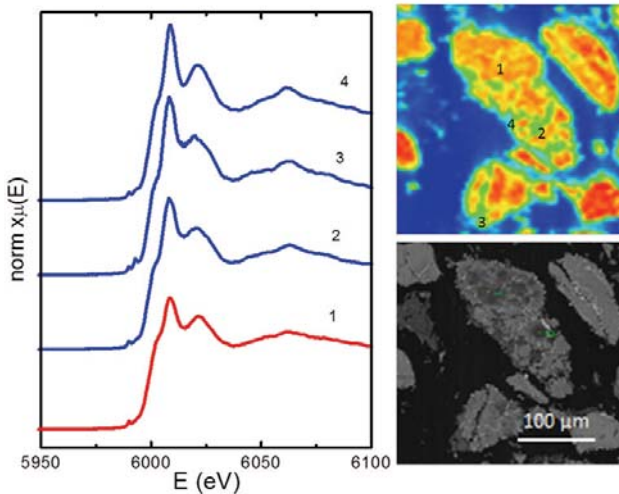

Figure 9—Normalized k³-weighted Cr K-edge micro-XANES spectra of residual chromite (no. 1 in red) and slag (nos. 2–4 in blue) resulting from direct reduction with NaOH at 1100°C for 1.5 hours. The map on the upper right represents Cr Kα micro-X-ray fluorescence showing the locations of the micro-XANES spectra, and the lower right is a backscattered electron photomicrograph of the same area.
(1): $NaAl_{0.40-0.45}Cr_{0.35-0.40}Fe_{0.2}O_2$; (2), (3), and (4): $NaAl_{0.7}Cr_{0.1}Fe_{0.1}O_2+SiO_2$

ferrochrome particles. The ferrochrome particles are largely unliberated or locked with the residual chromite and gangue particles. The degree of liberation clusters around the 20–40% range. This suggests that the liberation of ferrochrome at a coarse grind will be challenging and that the recovery of ferrochrome by conventional gravity and magnetic separation techniques would be limited.
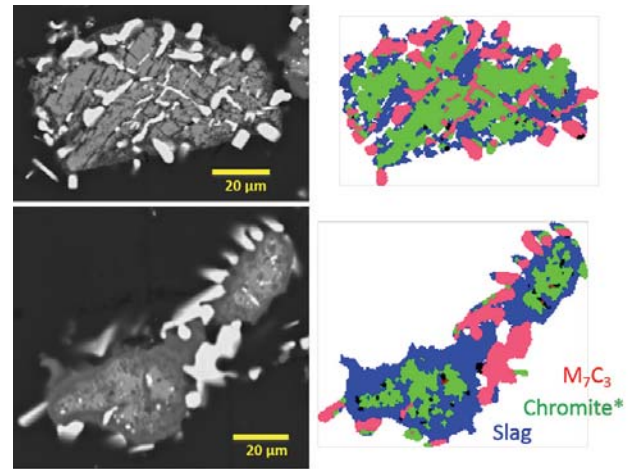

Figure 10—Backscattered electron images of reduced particles in the presence of NaOH and corresponding colour-coded drawings outlining individual phases measured by automated mineralogy. Composition of the residual chromite is different from that of the chromite in the original ore
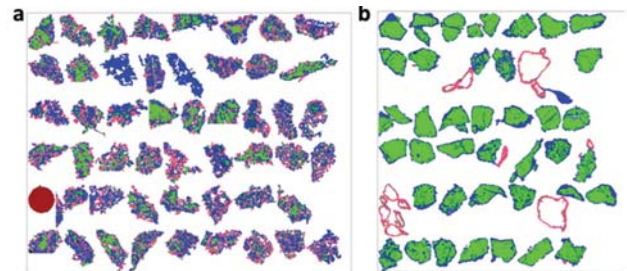

Figure 11—Distribution of alloy, slag, and residual chromite particles in the product formed from direct reduction in the presence of (a) NaOH and (b) NaCl. M_7C_3: pink; iron metal: red; slag: blue; residual chromite: green

As illustrated in Figure 11, the size of ferrochrome particles formed in the presence of NaCl is too small, suggesting that the degree of liberation would be less than satisfactory for typical mineral processing circuits. This is much improved in the case of NaOH-assisted reduction; however, the alloy particles are rather small. The particles are dominated by residual chromite, with much lower amounts of alloy and slag particles. These are detrimental to effective beneficiation of the alloy particles in the examples provided in this study.

Discussion

Alkali-assisted direct reduction of chromite results in various degrees of reduction and metallization, with Fe reduction always preceding that of Cr. In comparison to the 36% Cr metallization with no flux at 1300°C after 1 hour, it appears that NaCl addition slightly improved the Cr metallization to 45%. The degree of Cr metallization reached to 85% with the use of NaOH, and 66% with Na_2CO_3 as the flux.

It appears that the reduction and metallization of Cr and Fe species are localized along grain boundaries, microfractures, cleavage planes, and imperfections within chromite particles (Figure 4a–4d). With continued reduction,

Influences of alkali fluxes on direct reduction of chromite for ferrochrome production

Fe-rich Fe-Cr melt pools and segregates into larger immiscible liquid patches (Figures 2d, 4c, 4e, and 4f). Intricate spatial relationships among the alloy, residual chromite, and slag particles suggest that Fe is reduced *in situ* by CO whereas Cr is reduced on solid carbon particles. The alloys in the final product of NaOH reduction ($Cr_{4.2-4.6}Fe_{2.4-2.8}C_3$) are at a slightly lower degree of Cr metallization in comparison to the predicted alloy composition at equilibrium ($Cr_{4.8}Fe_{2.2}C_3$). In terms of Cr content, the individual alloy particles represent variable degrees of metallization, from 87.0 to 95.7% of the equilibrium value. These values are slightly higher than the observed degree of metallization, which is 85% based on the bulk XANES spectra of the final product. This discrepancy is reasonable considering the limited number of alloy particles analysed by electron microprobe and the uncertainty in the least-squares fitting of the XANES spectrum, which is about 5%. In the case of Na_2CO_3, compositions of the alloy particles, which are variable from $Cr_3Fe_4C_3$ to $Cr_4Fe_3C_3$ are indicative of Cr metallization varying from 61.5 to 82.7%, covering the observed degree of metallization at 66%. TGA measurements indicate mass losses of about 63% of the ore after 2 hours of reduction with 32% Na_2CO_3. When compared to the mass loss of about 41% with 12 % NaOH, these observations suggest that more Na_2CO_3 would be needed as the flux to achieve a similar degree of reduction as with NaOH. In addition, the CO_2 released from the decomposition of Na_2CO_3 would further retard the reduction. The compositions of the M_7C_3 type alloy particles formed under the influence of NaCl ($Cr_{3.2-5.0}Fe_{2.0-3.8}C_3$) indicate variable degrees of metallization in the 65.7 to 104.4% range, deviating from the equilibrium value. These numbers suggest non-equilibrium compositions for the alloy particles nucleated on graphite.

The products formed at 1300°C after 1 hour with NaCl flux are composed of chromite, graphite, Cr-Fe carbide, and olivine and are similar to those formed with no flux. At equilibrium, the quantities of alloy, spinel, and graphite forming at the temperature range of 800–1400°C in the presence of NaCl flux are similar to those formed without a flux (Figure 12a). Olivine contents forming at 800, 900, 1200, 1300, and 1400°C are also similar. The only

differences are in the Al-Si phases, which are cordierite ($Mg_2Al_4Si_5O_{18}$) and slag-liquid in the case of no flux and nepheline ($NaAlSiO_4$), feldspar ($NaAlSi_3O_8$), and slag-liquid in the case of NaCl flux. It appears that at low temperatures, there is little or no reaction between NaCl and chromite. The reaction products include nepheline, feldspar, and slag-liquid, some of which may have formed from the reactions with the gangue. The thermodynamics are in essence identical and NaCl has little influence on reduction and metallization.

In the presence of NaCl flux, predicted chromite compositions evolved, in part, towards increased Mg through the loss of Fe from the crystal structure, with little change in terms of the proportions of trivalent cations (Figure 3). In this case, with continued reduction Fe^{2+} would diffuse out towards the particle margins or reaction front. It is also possible that the Fe^{2+} ions are substituted by Mg released to the melt from the dissolution of clinochlore. The changes in the chromite composition were limited and occurred only after 1 hour of reduction, providing significant kinetic limitations to the reactions in accordance with the TGA results. In contrast, such changes in the residual chromite compositions were complete in the presence of NaOH and Na_2CO_3 fluxes. At equilibrium, the changes in the chromite composition are limited to increases in Mg due to reduction of Fe in the tetrahedral sites until 1100°C for the NaCl-assisted reduction (Figure 12b). Significant changes are predicted to occur in octahedral site occupancies above 1100°C. The mole fraction of Al increases by about 45% from 1100 to 1200°C (Figure 12b). This occurs at the expense of Cr in the octahedral sites, indicating significant Cr releases from the chromite structure in this temperature range. These cation distributions in chromite are similar to those occurring with no flux between 800 to 1400°C (Figure 12b). However, this does not necessarily mean that NaCl has no influence in accelerating the carbothermic reactions.

Our experimental findings and observations indicate that the role of NaCl in slag formation was also limited, likely due to its beginning to volatilize at around 1150°C. The TGA results indicate that NaCl melts around 800°C and evaporates at approximately 1150°C, which is in accordance with the empirical data (*i.e.* melting point being approx. 801°C and boiling point 1465°C)(Haynes, 2011). Furthermore, the NaCl slag has much higher MgO concentrations, at 29.4 and 33.2 wt%, and Cr_2O_3 concentrations at 6.2 and 13.7 wt%. Thermodynamic predictions indicate that the amount of liquid slag forming is very low, even at 1400°C. This would make NaCl not desirable as a flux. As discussed in our earlier publications, an effective accelerant must have a boiling point that is much higher and melting point that is lower than 1300°C, the optimum direct reduction temperature (Sokhanvaran and Paktunc, 2017a; Sokhanvaran, Paktunc, and Barnes, 2018; Yu and Paktunc, 2017, 2018a, 2018b).

The quantities of the main products forming at equilibrium in the presence of NaOH are shown in Figure 13a for the temperature range of 800–1400°C. The amounts of graphite remaining across the 800-1100°C range are relatively uniform, with a gradual decrease from about 14 to 13 wt% as the temperature increases. Across this temperature interval, the alloy is fcc-type Fe, increasing gradually in response to decreases of reductant. The amount of chromite/spinel remaining in the product across this
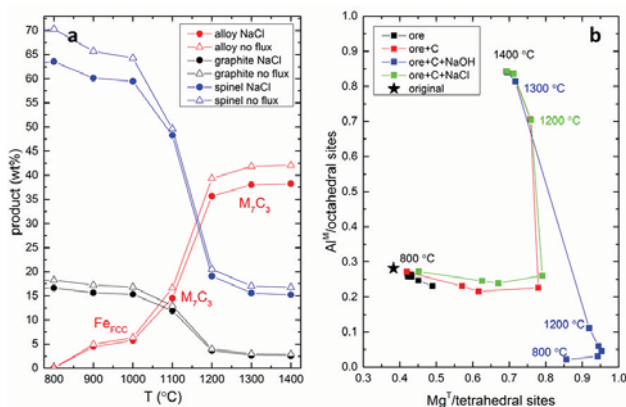

Figure 12—Thermodynamics of NaCl-assisted direct reduction during carbothermic reactions. (a) Equilibrium concentrations of chromite, graphite, and metallic phases predicted to form at 800 to 1400°C; (b) equilibrium partitioning of cations in the spinel structure at temperatures of 800 to 1400°C. 'Original': starting composition of chromite in ore

Influences of alkali fluxes on direct reduction of chromite for ferrochrome production
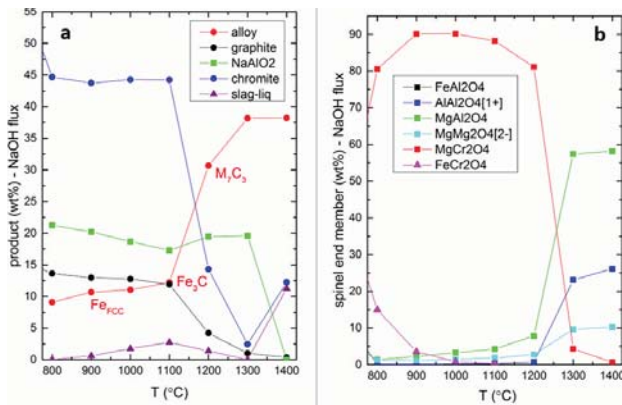

Figure 13—Thermodynamics of reduction aided by NaOH. (a) Equilibrium concentrations of chromite/spinel, graphite, metallic phases, NaAlO$_2$ phase, and slag-liquid predicted to form at 800 to 1400°C; (b) mass proportions of spinel end-members at temperatures of 800 to 1400°C under equilibrium

temperature interval is also uniform at about 45 wt%. Significant changes occur from 1100 to 1200°C, including a drastic decrease in the chromite/spinel content by about 30 wt%. Accompanying this change is the formation of M$_7$C$_3$ type carbide, reaching to about 32 wt%, and a sudden drop in the graphite content by about 8 wt%. This indicates that significant Cr reduction and metallization occur between 1100 and 1200°C. As chromite rapidly decomposes and is reduced by graphite, M$_7$C$_3$ alloy forms. At 1300°C, chromite is largely reduced to about 2 wt%. Another important compound forming in the case of direct reduction with NaOH is NaAlO$_2$. This phase is stable, and relatively abundant at about 20 wt% across the temperature interval of 800–1300°C (Figure 13a). NaAlO$_2$ is present as Na$_{0.9-1.2}$Cr$_{0.2-0.5}$Al$_{0.3-0.5}$Fe$_{0.0-0.3}$O$_2$ in the product formed at 1100°C. The source of Al in this case is the chromite, as discussed below. The product formed at 1300°C is composed of chromite, graphite, M$_7$C$_3$ type carbide, and a Na-Al silicate.

Thermodynamic simulations indicate that between 800 and 1200°C, the dominant chromite/spinel end-member is magnesiochromite (MgCr$_2$O$_4$), which is present at 80 wt% and higher (Figure 13b). Overall, chromite/spinel is depleted in Al. Thermodynamic simulations predict the formation of NaAlO$_2$ across this temperature range, including 1300°C. A small amount of Fe substitutes for Al in the structure. The presence of NaAlO$_2$ in the experimental products formed at 1100°C is confirmed by electron microprobe analyses and X-ray diffraction analyses. Its composition can be formulated as NaAl$_{0.40-0.45}$Cr$_{0.35-0.40}$Fe$_{0.2}$O$_2$. This phase has a layered structure with edge-sharing Al (and/or Cr and Fe) octahedra alternating with the close-packed Na octahedra in an edge-sharing form. These observations suggest that NaOH reacts with chromite to form NaAlO$_2$ and magnesiochromite across this temperature range. At 1200°C, the chromite composition is (Mg$_{0.9}$Al$_{0.1}$)(Cr$_{1.7}$Al$_{0.2}$Mg$_{0.1}$)O$_4$, becoming (Mg$_{0.7}$Al$_{0.3}$)(Cr$_{0.1}$Al$_{1.6}$Mg$_{0.3}$)O$_4$ at 1300°C. Essentially no reduction of Cr species occurs until 1100°C, and Cr is retained in the chromite (Figure 13b). Simulations indicate that NaAlO$_2$ becomes unstable after 1300°C. Following its

decomposition and with the release of Al, the refractory spinel (Mg$_{0.7}$Al$_{0.3}$)(Al$_{1.7}$Mg$_{0.3}$)O$_4$ forms at 1400°C.

It appears that the amount of Al$_2$O$_3$ released from the chromite is limiting the formation of slag liquid through the formation of NaAlO$_2$. The Cr species in the slag, which is dominated by Na(Cr,Al,Fe)O$_2$, is trivalent, occurring in six-fold coordination to oxygen (Figure 9). This suggests that Cr is transported as small polymeric species in the molten/liquid slag. This highlights the importance of NaAlO$_2$ in limiting the formation of slag-liquid and the transport of Cr species. This is analogous to our findings for CaCl$_2$ (Yu and Paktunc, 2017, 2018a, 2018b) and waste material (Sokhanvaran and Paktunc 2017) in that the formation of a molten medium in the temperature range 800–1400°C is crucial for effective collection and reduction of the Cr and Fe species. It is predicted that the amount of slag-liquid forming at 800–1300°C under equilibrium conditions is very low, not exceeding 2.7 wt%. This increases to 11.3 wt% at 1400°C, suggesting that NaOH-assisted direct reduction would require temperatures higher than 1300°C. For an effective reduction and segregation of ferrochrome from the residual slag, as in the case of CaCl$_2$-assisted direct reduction (Yu and Paktunc, 2018a, 2018b), the reducible cations (i.e. Cr^{3+} and Fe^{2+}) should be transported as ionic species in the form of monomers, dimers, or small oligomeric species in molten media or a gas phase and reduced on carbon particles.

Conclusions

Direct reduction of chromite ore with alkali fluxes at 1300°C for 1 hour produced (Cr,Fe)$_7$C$_3$ type alloys with Cr/Fe mass ratios variable from 0.7 to 2.3. Among the alkali fluxes, NaCl resulted in a low degree of Cr metallization, at 45%. This is largely due to evaporation of NaCl at around 1150°C. Reduction with Na$_2$CO$_3$ resulted in 66% Cr metallization. NaOH caused a much higher degree of Cr metallization, reaching 85% with the ferrochrome alloy being Cr$_{4.2-4.6}$Fe$_{2.4-2.8}$C$_3$ and having a Cr/Fe mass ratio of 1.4–1.8.

Metallization is facilitated by the formation of liquid slag in the presence of Na$_2$O and Al$_2$O$_3$. The Cr and Fe oxides are transported in the liquid slag as ionic species to the reduction sites on solid carbon particles. The details of the reaction mechanism will be presented in a separate paper. Across the temperature range of 800–1200°C, NaOH reacts with chromite to form NaAlO$_2$ and magnesiochromite, which is (Mg$_{0.9}$Al$_{0.1}$)(Cr$_{1.7}$Al$_{0.2}$Mg$_{0.1}$)O$_4$ at 1200°C. Magnesiochromite becomes unstable at 1300°C, resulting in the release of Cr. However, NaAlO$_2$ is still stable, which limits the formation of liquid slag. This is detrimental to collecting and transporting the charged octahedral CrO$_6$ species in molten media to graphite particles. Following the decomposition of NaAlO$_2$ above 1300°C, the amount of liquid slag increases to about 12 wt% at 1400°C and a refractory Mg-Al spinel forms.

Ferrochrome particles formed under the limited experimental conditions studied in this paper at 1300°C and lower are small and largely unliberated. This would make the recovery of ferrochrome by conventional gravity and magnetic separation techniques difficult. It appears that the NaOH-assisted direct reduction and alloy growth would require reduction temperatures greater than 1300°C and effective transport of reducible cations in a molten medium or gas phase to carbon particles.

Influences of alkali fluxes on direct reduction of chromite for ferrochrome production

With a degree of metallization of 85%, direct reduction of chromite aided by NaOH is promising as an alternative technology to conventional smelting in electric arc furnaces or as a prereduction technology prior to conventional smelting. Based on our extensive review of furnaces used for direct reduction of iron and the work of Sokhanvaran, Paktunc, and Barnes (2018), it is envisaged that rotary kiln- and rotating hearth-type furnaces would be potentially suitable for direct reduction of chromite. There is the potential for the formation of Cr^{6+} in the presence of excess oxygen during reduction. This and other waste management issues related to direct reduction of chromite are being investigated.

References

Barnes, A., Muinonen, M., and Lavigne, M.J. 2015. Reducing energy consumption by alternative processing routes to produce ferrochromium alloys from chromite ore. *Proceedings of the Conference of Metallurgists, Annual Meeting, COM* 2015. CIM, Montreal. 22 pp.

Beukes, J.P., Van Zyl, P.G., and Neizel, B.W. 2015. Process for enhanced pre-reduction of chromite. Patent WO2015015250 A1.

Dawson, N.F. and Edwards, R.I. 1986. Factors affecting the reduction rate of chromite. *INFACON 86: Proceedings of the 4th International Ferro-alloys Congress*, Rio de Janeiro, Brazil, 31 August - 3 September. Finardi, J., Nascimento; J.O., and Homem de Melo, F.D. (eds.). Associacao Brasileira dos Produtores de Ferro-Ligas-Abrafe, Sao Paulo. pp.105–113.

Haynes, W.M. 2011. CRC Handbook of Chemistry and Physics (92nd ed.). CRC Press. ISBN 978-1439855119Haynes, W.M. 2014. CRC *Handbook of Chemistry and Physics*. 94th edn. CRC Press, Boca Raton, FL. pp. 4–89

International Chromium Development Association. 2016. Life cycle inventory (LCI) of primary ferrochrome production 2012. Final Report. 48 pp.

Katayama, H.G., Tokuda, M., and Ohtani, M. 1986. Promotion of the carbothermic reduction of chromium ore by the addition of borates. *Transactions of the Iron and Steel Institute of Japan*, vol. 22, no. 10. pp. 1513–1520.

Lekatou, A. and Walker, R.D. 1997. Effect of SiO_2 addition on solid state reduction of chromite concentrate. *Ironmaking & Steelmaking*, vol. 24. pp. 133–143.

Mccullough, S., Hockaday, S., Johnson, C., and Barcza, N.A. 2010. Pre-reduction and smelting characteristics of Kazakhstan ore samples. *INFACON 2010: Proceedings of the12th International Ferroalloys Congress: Sustainable Future*, Helsinki, Finland, 6–9 June. Vartiainen, A. (ed.). Outotec Oyj. pp. 249–262.

Naiker, O. 2007. The development and advantages of Xstrata's Premus process. *INFACON XI: Proceedings of the 11th International Ferroalloys Congress: Innovation in Ferroalloy Industry*, New Delhi, India, 18–21 February. Indian Ferro Alloy Producers Association. pp. 112–119.

Naiker, O. and Riley, T. 2006. Xstrata Alloys in profile. *Proceedings of Southern African Pyrometallurgy*, Johannesburg, South Africa. Jones, R.T. (ed.). Southern African Institute of Mining and Metallurgy, Johannesburg. pp. 297–306.

Neizel, B.W., Beukes, J.P., Van Zyl, P.G., and Dawson, N.F. 2013. Why is $CaCO_3$ not used as an additive in the pelletised chromite pre-reduction process? *Minerals Engineering*, vol. 45. pp. 115–120.

Niayesh, M.J. and Fletcher, G.W. 1986. An assessment of smelting reduction processes in the production of Fe–Cr–C alloys. *Proceedings of the 4th International Ferroalloys Congress*, Rio de Janeiro, Brazil, 31 August - 3 September. Finardi, J., Nascimento, J.O., and Homem de Melo, F.D. (eds.). Associacao Brasileira dos Produtores de Ferro-Ligas-Abrafe, Sao Paulo, Brazil. pp. 115–123.

Nunnington, R.C. and Barcza, N.A. 1989. Pre-reduction of fluxed chromite-ore pellets under oxidizing conditions. *Proceedings of the 5th International Ferroalloys Congress*, New Orleans, USA, 23–26 March. Oxaal, J.G. and Downing, J.H. (eds.). Ferroalloys Association, Arlington, VA. pp .55–68.

Paktunc, D. 2001. MODAN - a computer program for estimating mineral quantities based on bulk composition: Windows version. *Computers and Geosciences*, vol. 27. pp. 883–886.

Paktunc, D. 2004. A computer program for analysing complex bulk XAFS spectra and for performing significance tests. *Journal of Synchrotron Radiation*, vol. 11. pp. 295–298.

Ravel, B. and Newville, M. 2005. Athena, Artemis, Hephaestus: data analysis for X-ray absorption spectroscopy using IFEFFIT. *Journal of Synchrotron Radiation*, vol. 12. pp. 537–541.

Riekkola-Vanhanen, M. 1999. Finnish expert report on best available techniques in ferrochromium production. The Finnish Environment 314, Environmental Protection, Helsinki, Finland.

Sokhanvaran, S. and Paktunc, D. 2017a. Carbothermic reduction of chromite ore using an industrial waste as the additive. Patent application. PCT/CA2017/051252 and US 15/788,953, 20 October 2017.

Sokhanvaran, S. and Paktunc, D. 2017b. The effect of fluxing agent on direct reduction of chromite ore. *Proceedings of the Conference of Metallurgists, COM'2017*. Canadian Institute of Mining, Metallurgy and Petroleum, Montreal. 13 pp.

Sokhanvaran, S., Paktunc, D., and Barnes, A. 2018. NaOH–assisted direct reduction of Ring of Fire chromite ores, and the associated implications for processing. *Journal of the Southern African Institute of Mining and Metallurgy*, vol. 118. pp. 581–588.

Takano, C., Zambrano, A.P., Nogueira, A.E.A., Mourao, M.B., and Iguchi, Y. 2007. Chromite reduction reaction mechanisms in carbon–chromite composite agglomerates at 1773 K. *ISIJ International*, vol. 47. pp. 1585–1589.

Van Deventer, J.S.J. 1988. The effect of additives on the reduction of chromite by graphite. *Thermochimica Acta*, vol. 127. pp. 25–35.

Wang, Y., Wang, L., and Chou, K.C. 2015. Effects of CaO, MgO, Al_2O_3 and SiO_2 on the carbothermic reduction of synthetic $FeCr_2O_4$. *Journal of Mining and Metallurgy*, Section B: Metallurgy, vol. 51. 8 pp.

Weber, R, P. and Eric, R.H. 1992. Solid state fluxed reduction of LG-6 chromite from the Bushveld Complex. *Proceedings of the 6th International Ferroalloys Congress*, Cape Town, South Africa. Southern African Institute of Mining and Metallurgy, Johannesburg. pp. 71–77.

Winter, F. 2015. Production of chromium iron alloys directly from chromite ore. Patent WO2015/060951.

Yu, D. and Paktunc, D. 2017. Carbothermic direct reduction of chromite using a catalyst for the production of ferrochrome alloy. Patent application, PCT/CA2017/050923 - 2017-08-02; US application 62/500,147.

Yu, D. and Paktunc, D. 2018a. Direct production of ferrochrome by segregation reduction of chromite in the presence of calcium chloride. *Metals*, vol. 8, no. 1. p. 69. https://doi.org/10.3390/met8010069

Yu, D. and Paktunc, D. 2018b. Calcium chloride-assisted segregation reduction of chromite: influence of reductant type and the mechanism. *Minerals*, vol. 8, no. 2. p. 45. https://doi.org/10.3390/min8020045

Yu, D. and Paktunc, D. 2018c. Kinetics and mechanisms of the carbothermic reduction of chromite in the presence of nickel. *Journal of Thermal Analysis and Calorimetry*, vol. 132, no. 1. pp. 143–154. https://doi.org/10.1007/s10973-017-6936-6 ◆